CrossMark

RESEARCH PAPER

Effect of welding speed on mechanical and fracture behavior of nitinol laser-joints

Ali Shojaei Zoeram[1] · Ali Asghar Akbari mousavi[1] · Farhad Mohsenifar[2]

Abstract In this study, the effect of a pulsed Nd:YAG laser speed welding of Nitinol plates on the microstructure, mechanical properties and fracture behavior was investigated. The samples were double-sided butt welded in various welding speeds. Optical and Scanning Electron Microscopy, EDS analysis, XRD, microhardness and tensile test were used for the weldment characterization. Under the circumstances in which the heat input was low, the amount of Ti2Ni brittle intermetallic phase in the weld metal was reduced and this removed brittle grain boundaries from weld metal and consequently improved mechanical properties. Investigations on the fracture surfaces of the tensile test specimens showed that fracture mechanism was changed by increase of the welding speed.

1 Introduction

Properties such as shape memory behavior, super elasticity, corrosion resistance, and biocompatibility have turned

✉ Ali Shojaei Zoeram
a.shojae@alumni.ut.ac.ir

1 Welding Lab, School of Metallurgy and Materials, College of Engineering, University of Tehran, PO Box 11155-4563, Tehran, Iran

2 Mechanical Engineering Department, Higher Education Complex of Bam, Po Box 76613-14477, Bam, Kerman, Iran

nitinol alloy into unique alloy with special applications [1–5]. Although these unique properties of nitinol have been discovered since 1960 [6], but due to problems associated with poor formability and welding, this alloy has not found its proper position among the designers and manufacturers [7, 8]. Formation of Ti_2Ni and Ni_3Ti brittle intermetallic phases in weld metal of Ti-rich and Ni-rich alloys, respectively, is the main problem associated with welding of this kind of alloys [9–11]. Due to non-equilibrium effects the titanium-rich alloys are subjected to precipitation of Ti_2Ni particles during solidification. Indeed, while cooling, segregation of titanium can lead to the formation of richer liquid clusters, which may finally solidify as Ti_2Ni precipitates located at grain boundaries. Precipitations of this brittle intermetallic phase may severely impair mechanical properties of this alloy, because they act as crack initiation sites [12]. Increase of solidification rate has a positive role on reduction of amount of deposited intermetallic phase in weld metal [13]. Therefore, due to a higher solidification rate in laser welding methods, [14] this welding method is very promising for welding this class of metals which are sensitive to formation of brittle phases due to welding. Both of CO2 gas laser [15] and Nd:YAG solid state laser [16–18] have been used for welding nitinol shape memory alloy. In particular the Nd:YAG source is suitable for welding low-thickness components due to an accurate control of the welding power, resulting in a reduced heat-affected zone (HAZ) [19]. Therefore in this study a pulsed Nd:YAG source was used to welding of NiTi/NiTi joints.

Equation 1 represents the amount of heat input per unit length of the weld (J/mm) in pulsed laser welding [20]. In this equation E_p is the energy from each pulse in (J), f is the frequency in (Hz), V is the welding speed in (mm/s) and P_{av} is the average pulsed energy.

Springer

Heat Input per unit length of the weld

$$\left(\frac{J}{mm}\right) = \frac{P_{av}}{V} = \frac{E_P(J)*f(Hz)}{V\left(\frac{mm}{s}\right)} \qquad (1)$$

According to Eq 1, increasing the welding speed in pulsed laser welding leads to the reduction of the amount of heat input per unit length of the weld and this gives rise to increase the weld metal solidification rate [21]. Regarding the relationship between the increase of solidification rate and reduction of precipitation of intermetallic phase in weld metal [13] in this study, the effects of welding speed on the microstructure, mechanical properties, and fracture behavior was investigated.

2 Experimental procedure

In order to produce Ti-rich Nitinol plates with chemical composition of (Ni–50.7 at.%Ti) and thickness of 1 mm, high pure nickel and titanium with a specified weight ratio were casted in a Vacuum Arc Re-melting (VAR) furnace. The casted ingot with a thickness of 1 cm was successfully roll-formed in sequential hot and then cold situations using low-loads. Rolling procedure was designed so that 20 % of the overall thickness reduction was dedicated to cold forming. To eliminate cold work, sheets were annealed in 450 °C for 30 min and then quenched in water bath. A black oxide layer formed during the previously mentioned procedure was removed with an acid mixture solution of HF: HNO_3: H_2O=1:5:10. The laser welding tests were carried out with an SW-1 pulsed Nd:YAG laser machine with the maximum average power of 100 W and wavelength of 1.064 μm. Used welding parameters for welding of samples are given in Table 1. According to Fig. 1, the double-sided welding method was used for welding of all samples. All the samples were welded at the voltage of 480 V, the defocusing distance of −0.6 mm, frequency of 8.2 Hz and beam diameter of 0.4 mm and with the protection of argon atmosphere with flow rate of 7 L/min.

Etching process was performed by immersion of the samples in the solution of HF:HNO_3:H_2O 1:4:5 and exposure time of 20 s.

The OM and SEM was used to analyze the microstructure of the welded joints. X-ray diffraction (XRD) analysis was carried out on fracture surfaces of tensile samples for identification of the formed phases in the weld metal and EDS
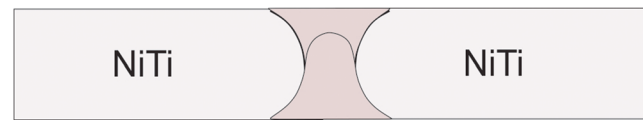
Fig. 1 Double-sided welding method

analysis performed on fracture surfaces in order to verifying the X-ray diffraction results. Moreover, to evaluate the hardness change through the weld metal, Microhardness profiles were attained on transverse sections of the specimens using a load of 200 g for 15 s. Mechanical properties of the joints were evaluated via tensile tests with strain rate of 1 mm/min at room temperature on two samples of each welding speed. Dimensions of the tensile test specimen are given in Figs. 2 and 3.

3 Results and discussion

3.1 Microstructure of welded joints

The G/R ratio determines the morphology of a solidification structure, where, G is the temperature gradient and R represents the growth rate [21]. According to Eq (1), the heat input decreases with increasing welding speed. The lower the heat input leads to the higher the temperature gradient G and hence the higher the ratio G/R [21]. Therefore, at lower heat inputs, G/R is higher and columnar solidification prevails [21]. According to Fig. 4a, the microstructure of weld metal is composed of the columnar and equiaxed dendritic microstructures. The width of these regions is affected by the welding parameters. According to Eq. 1, increasing the welding speed decreases heat input and consequently, G/R ratio increases according to Fig. 4 in this condition columnar solidification prevails [21]. Figure 4b and c illustrate the microstructures of weld metals which were welded under 1.25 and 1.75 mm/s welding speeds, respectively. As shown in Table 1, with increasing welding speed from 1.25 to 1.75 mm/s heat input decreases from 39.4 to 28.1 J/mm and the length of columns increased from 65.5 to 128 μm (Fig. 4b, c). Segregation of Titanium in Ti-rich nitinol alloys during solidification leads to formation of Ti-rich liquid clusters in weld metal which can eventually solidify as Ti_2Ni phase in grain boundaries that makes the grain boundaries more brittle [12]. On the other hand, increasing the heat input as a result of decreasing the welding speed leads to increasing the volume of fusion metal

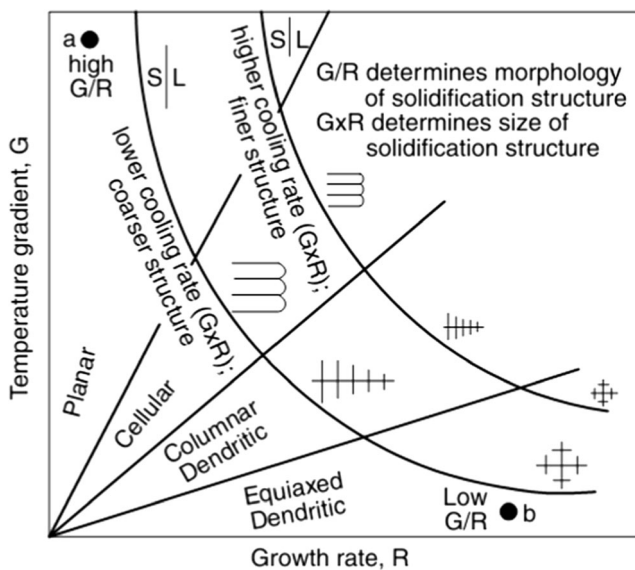| Table 1 Used parameters for welding of joints					
Sample No	E_P (J)	Pulse duration (ms)	Frequency (Hz)	Welding speed (mm/s)	Heat input (J/mm)
1	6	2	8.2	1.25	39.4
2	6	2	8.2	1.50	32.8
3	6	2	8.2	1.75	28.1

Fig. 2 Dimensions of tensile test samples
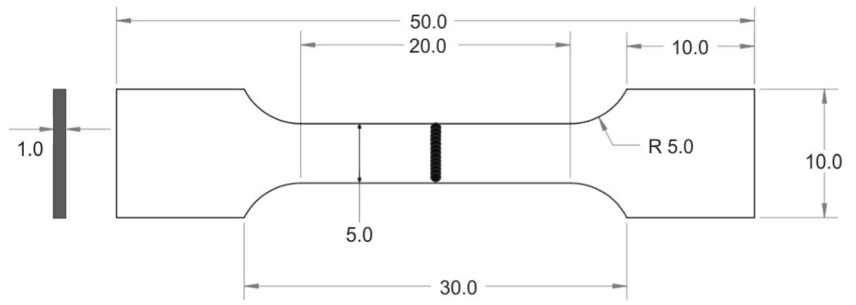
and consequently, increases of applied tensile stresses during solidification progress to weld metal. More precipitation of Ti_2Ni in grain boundaries and much tensile stress in welded samples with higher heat input during contraction lead to formation of solidification cracks in weld metals of samples which welded with lower welding speed. Fig. 5 shows the typical solidification cracking in weld metal.

As can be seen in Fig. 6 partial melted zone is observed immediately outside the weld metal. The presence of dark-etching GBs along the fusion boundary in Fig. 6 is an indication of GB liquation. As mentioned used alloy in present study was a Ti-rich nitinol alloy, therefore grain boundaries of this alloy are exposed to precipitation of Ti_2Ni phase during steps in the production of nitinol plates. According to binary phase diagram (Fig. 7); melting zone of this phase is lower than NiTi (984 °C) and heat from welding could leads to melting of this phase in heat-affected zones (Fig. 6).
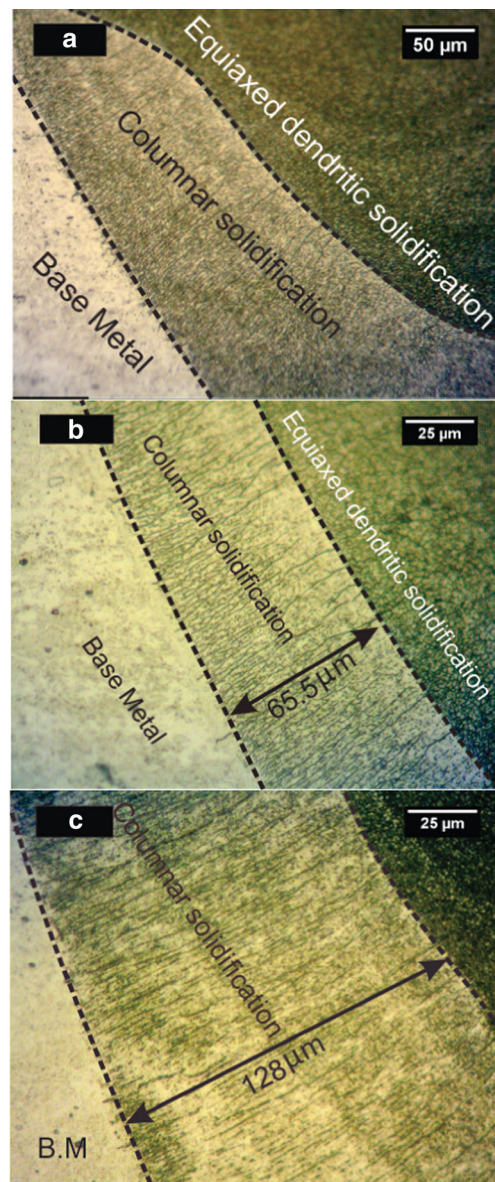
3.2 X-ray diffraction analysis

The formation of Ti_2Ni phase in grain boundaries of the weld metal severely impairs mechanical properties of NiTi/NiTi

joints. The used alloy in this study was a titanium-rich alloy. According to phase diagram (Fig. 7) the Ti_2Ni could be formed as result of NiTi+liquid⇒Ti_2Ni peritectic reaction

Fig. 4 Effect of welding speed on the microstructure of weld metal (**a**) typical microstructure of weld metal (**b**) 1.25 mm/s (**c**) 1.75 mm/s

Fig. 3 Effect of temperature gradient G and growth rate R on the morphology and size of solidification microstructure

Fig. 5 Solidification cracking in center areas of weld metal with equiaxed microstructure welded sample with 1.25 mm/s
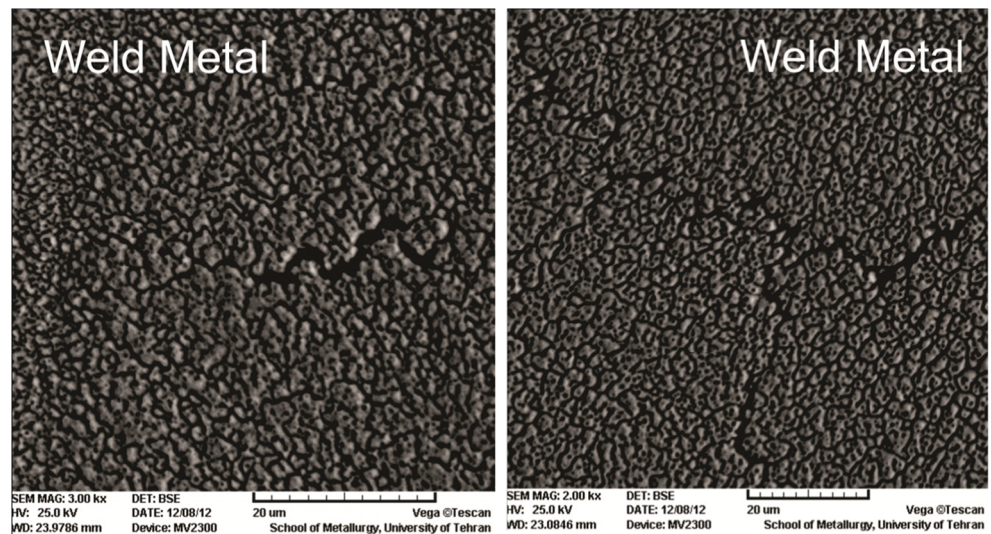
and accumulates in grain boundaries of weld metal [12]. The intensity of a peak I_{hkl} is given by:

$$F_{hkl} = \sum_{i=1}^{n} f_i \exp 2\pi(hx_i + ky_i + lz_i) \quad I_{hkl} \propto |F_{hkl}|^2$$

Where the structure factor, F_{hkl}, of a reflection, hkl, is dependent on the type of atoms and their positions (x, y, and z) in the unit cell.

$$F_{hkl} = \sum_{i=1}^{n} f_i \exp 2\pi(hx_i + ky_i + lz_i)$$

f_i is the scattering factor for atom i and is related to its atomic number.

Therefore, the peak intensity related to the sum of reflecting plates, i.e., amount of that special phase. Therefore, the peak intensities are related to the amount of each phase present in the sample.

Hence, in order to assess the effect of welding speed on formed intermetallic phases in the weld metal and identify them, X-ray diffraction analysis was performed on fracture surface of tensile samples. Figure 8 illustrates the results of X-ray diffraction analysis. It is obvious that increasing the welding speed decreases the peak intensity corresponding to Ti_2Ni phase.

Reduction of the magnitude of this intermetallic phase in the weld metal due to increase of welding speed, could be as a direct result of the reduction of the available time for the peritectic chemical reaction of NiTi+liquid⇒Ti_2Ni, because increasing the welding speed increase solidification rate [22].

Fig. 6 PMZ of Ti-rich nitinol
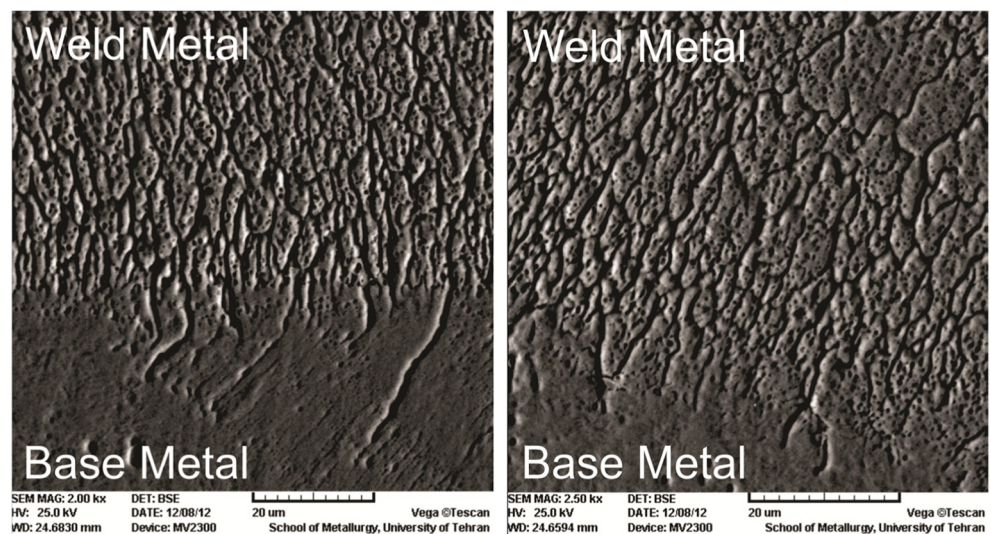
Fig. 7 Ni-Ti binary phase diagram
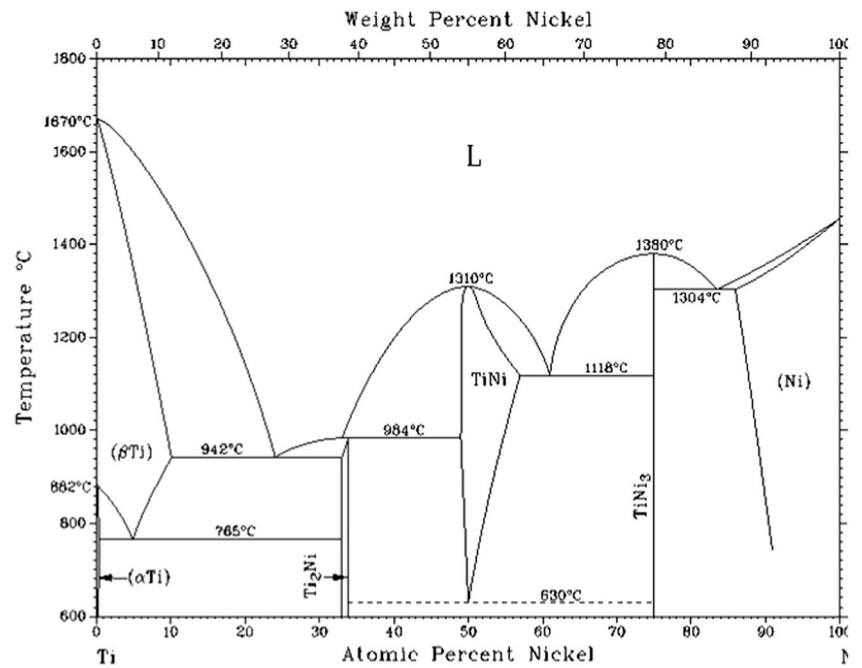
3.3 Mechanical properties

3.3.1 Hardness

Microhardness profile of this joint is given in Fig. 9. As can be seen, the weld metal hardness is harder than the base metal. This was justified by the observed intermetallic Ti_2Ni phase in weld metal according to result of XRD patterns this increase.

3.3.2 Mechanical behavior

Mechanical behavior of welded samples is shown in Fig. 10a, b. The results show that the welding parameters have a great influence on the mechanical behavior of joints; so that for the welding speed increase from 1/25 to 1.75 mm/s, the tensile strength of the joints increased about 104 %. By comparing

the results of the tensile tests and the X-ray diffraction analysis of fracture surfaces (Fig. 8), a direct relation between the peaks intensity corresponding to Ti_2Ni intermetallic compound and the reduction of tensile strength of joints is observed. Figure 10 shows the highest tensile strength is obtained under the circumstances that the peak intensity of the Ti_2Ni intermetallic compound decreases. This could be obtained by increasing the welding speed.

3.4 Fracture surface

The fracture surface of sample 1 which was welded with higher heat input is given in Fig. 11. As can be seen, the fracture surface of this sample can be divided into two parts of smooth and rough areas based on amount of roughness. According to the phase diagram of TiNi, Ti_2Ni is the product

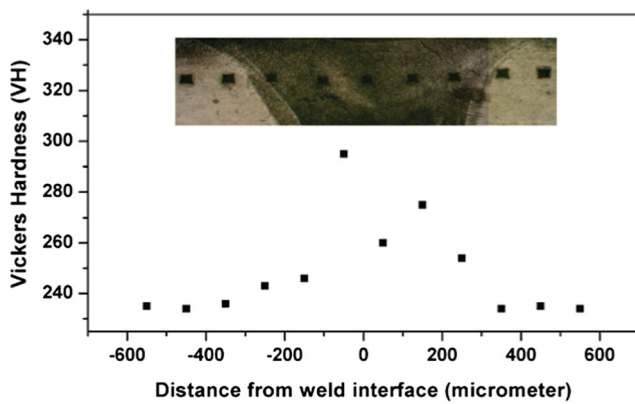**Fig. 8** X-ray patterns of fracture surfaces
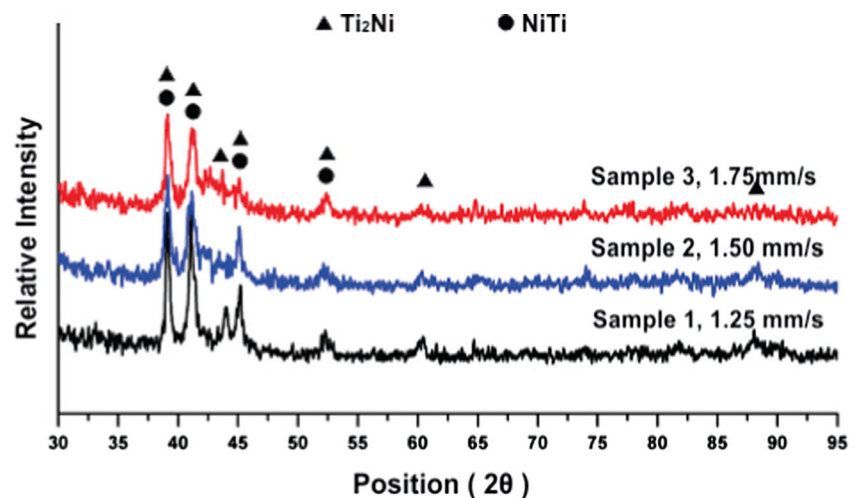
Fig. 9 Microhardness profile of joint

Fig. 11 Fracture surface of sample 1

of a peritectic reaction (Fig. 7) [23]. The peritectic reaction products accumulate in the grain boundaries (Fig. 13). Accumulation of a brittle Ti_2Ni phase in the grain boundaries creates a brittle path, which is very suitable for initiation and progression of cracks (Fig. 12). As noted weld metal microstructure consists of columnar and equiaxed areas, therefore crack propagation on route 1 (grain bounders of columnar
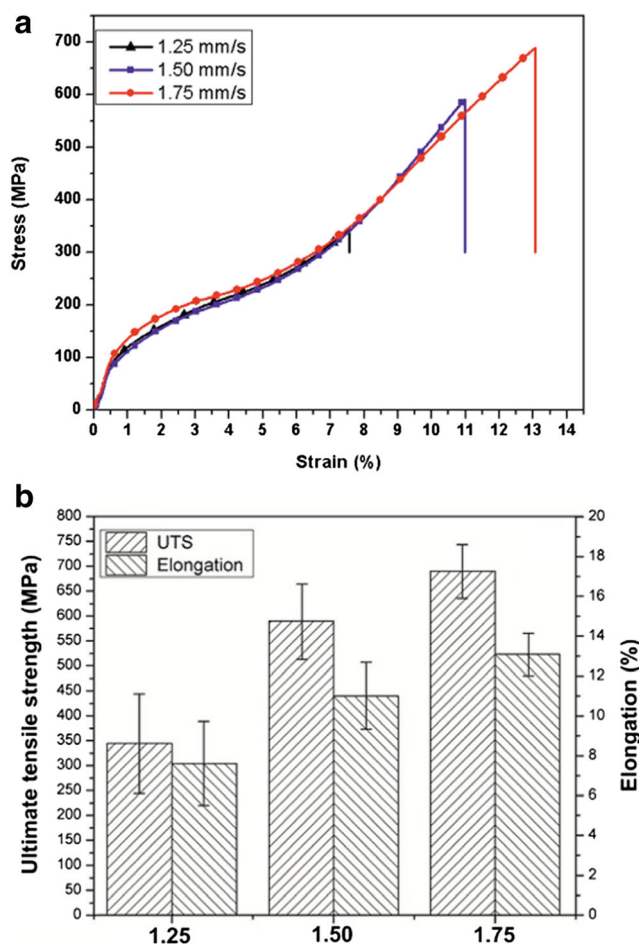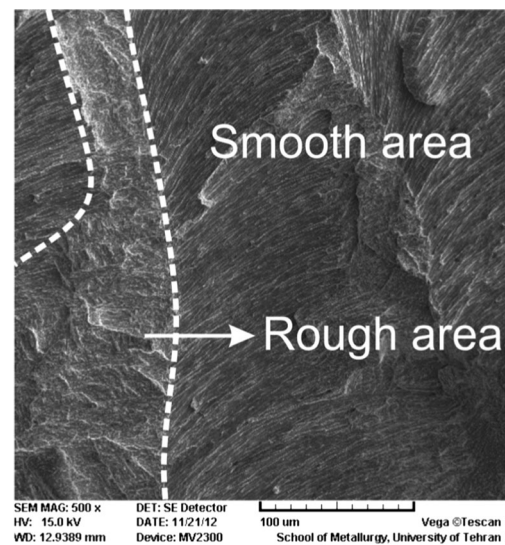
microstructure) in Fig. 12 leads to the formation of smooth areas, and on the other hand, crack propagation on route 2 (equiaxed areas) leads to formation of rough area in fracture surface of sample 1 (Fig. 11).

The SEM images of fracture surfaces of laser-welded joints with different welding parameters are shown in Fig. 14. As can be seen, changes in welding parameters could somewhat change the mechanism of fracture. Fig. 14a–c shows the fracture surface for the pulse duration of 2 ms, frequency of 8.2 Hz and welding speed of 1.25 mm/s condition, which exhibited lowest tensile strength among tensile samples (Fig. 10). In this situation, a smooth fracture surface that shows the directional dendritic solidification microstructure of the weld is observed. This is an indicative of intergranular failure where the fracture propagates along grain boundaries of the columnar microstructure. Since XRD analysis was performed on the fracture surface which peak intensity corresponded to Ti_2Ni for this sample is higher and regarding the fracture surface of this sample which is almost transgranular, cause of this phenomenon is accumulation of Ti2Ni brittle intermetallic phases in these areas. In contrast, the sample that was welded in the condition of pulse duration of 2 ms, frequency of 8.2 Hz and welding speed of 1.5 mm/s (Fig. 14d–f), revealed a relatively coarser fracture surface. With increasing welding speed,

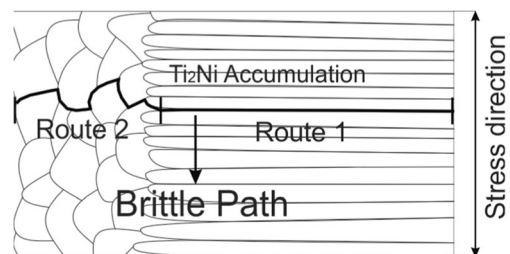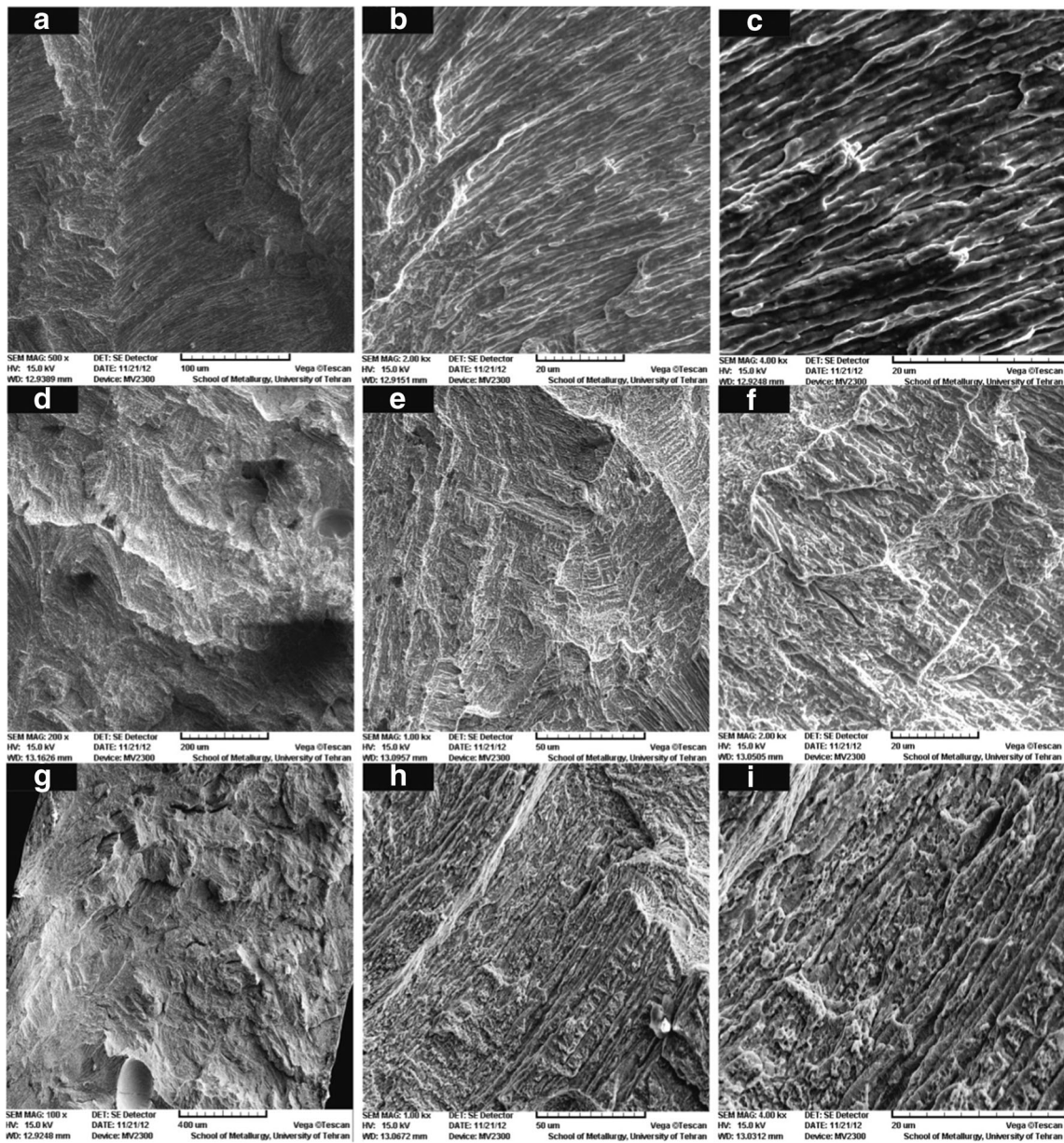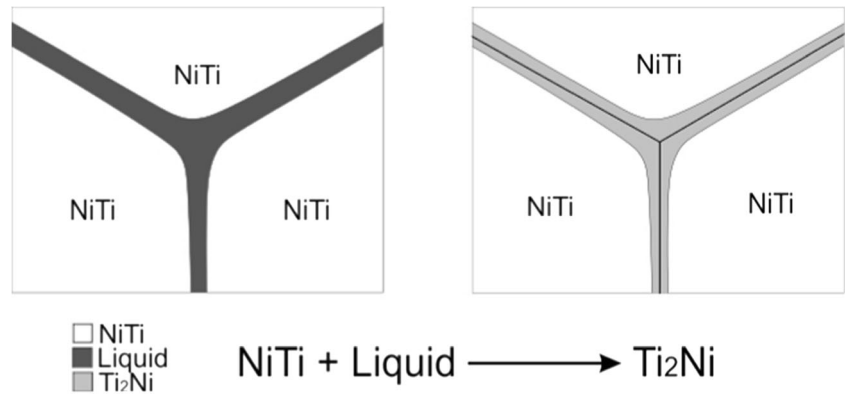Fig. 10 Effect of welding speed on mechanical behavior of welded joints

Fig. 13 Suggested crack initiation site and its propagation path

Fig. 12 Accumulation of Ti$_2$Ni in grain boundaries

Fig. 14 Effect of welding speed on fracture behavior (a–c) 1.25 mm/s (d–f) 1.50 mm/s (g–i) 1.75 mm/s

changing the failure mechanism is more intuitive. As was shown in stress–strain curves in Fig. 10, the sample no. 3 that was welded with lower heat input had the highest tensile strength and elongation. In fracture surface related to this sample the features corresponding to directional dendritic solidification microstructure that shows intergranular fracture is largely eliminated, and instead, the areas containing the dimples was added to the fracture surface (Fig. 14h). Therefore, the fracture surface of this sample is a combination of transgranular and intergranular areas, sections related to transgranular contain dimples. Dimples increases fracture surface roughness (Fig. 14g). In other words, dimple appearance presents increase of welding speed, eliminates the brittle path, and changes the failure mechanism from intergranular with a lower elongation to relatively ductile failure with a higher elongation (Fig. 10). By comparing Fig. 14c and i that related to fracture surface of sample 1 and 3, respectively, in high magnification, this changing in failure mechanism is more tangible. In Fig. 14c, only the characteristics of intergranular failure are observed; while in Fig. 14i, dimples in the fracture surface can be observed that represents a ductile failure. As mentioned, precipitated Ti_2Ni phase in weld metal acts as initiation crack sites and deteriorates mechanical properties of joints [12]. According to XRD results (Fig. 8), increase of welding speed decreases the peak intensity related to the phase of Ti_2Ni. This phase is product of a peritectic reaction and form brittle grain boundaries. Therefore with increase of welding speed amount of deposited Ti_2Ni phase in grain boundaries is decreased, brittle grain boundaries are eliminated and fracture mechanism changes to transgranular and this improves mechanical properties of joints (Fig. 10).

3.5 EDS Analysis of fracture surface

Average EDS analysis of fracture surfaces of tensile specimens shows titanium content of weld metal decreases with increasing the welding speed (Fig. 15). As can be seen, the tensile strength of the samples is directly dependent on the titanium to nickel ratio. Results of EDS analysis confirms results of X-Ray diffraction analysis that showed peak intensity corresponded to Ti_2Ni phase is reduced with increase of welding speed. This leads to a change of the fracture mechanism from intergranular to transgranular and improvement of mechanical properties due to increase of welding speed.

4 Conclusion

Welding parameters have considerable effects on the mechanical properties of NiTi/NiTi joint. The main reason for the deterioration of the mechanical properties of welded joints is the precipitation of the Ti_2Ni brittle intermetallic phase in weld metal. This brittle phase is a result of a peritectic reaction, which products' accumulate in the grain boundaries and leads to their brittleness, intergranular fracture, and consequently, the decline in mechanical properties. The study showed that one method to improve the mechanical properties of the welded joints is the reduction of the magnitude of the Ti_2Ni intermetallic phase in weld metal. This can be achieved with an increase in the welding speed.. Results of X-ray diffraction and EDS analysis performed on fracture surfaces showed that: an increase of the welding speed leads to reduction precipitation of Ti_2Ni phase in weld metal. According to results from survey of fracture surface reduction of precipitation of TI_2Ni

Fig. 15 Correlation between Ti/Ni ratio and ultimate fracture stress of tensile samples
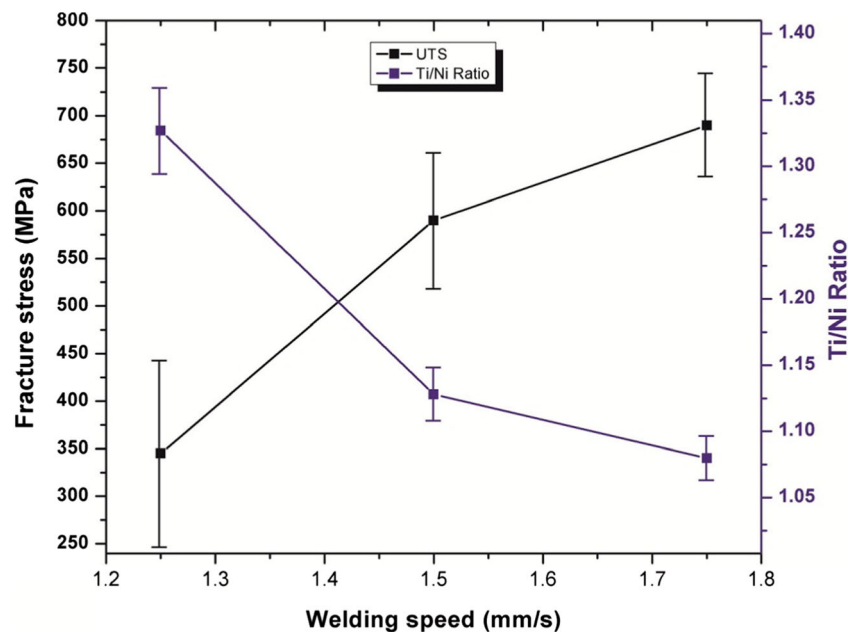
phase leads to removing the brittle path and this improves mechanical properties.

References

1. Miyazaki S, Otsuka K, Suzuki Y (1981) Transformation pseudoelasticity and deformation behaviour in a Ti-50.6 at % Ni alloy. Scr Metall 15:287–292
2. Miyazaki S, Igo Y, Otsuka K (1986) Effect of thermal cyclic deformation on the pseudoelasticity characteristics of Ti-Ni alloys. Acta Metall 34:2045–2051
3. Sabur T, Yoshida M, Nenno S (1984) Deformation behaviour of shape memory Ti-Ni alloy crystals. Scr Met Mater 18:363–366
4. Takei F, Miura T, Miyazaki S (1983) Stress-induced martensitic transformation in a Ti-Ni single crystal. Scr Metall Mater 17: 987–992
5. Zhi CL, Xing KZ, Hong Z (2003) Microstructure and superelasticity of severely deformed TiNi Alloy. Mater Lett 57:1086–1090
6. Buehler WJ & Wiley RC (1965) Nickel base alloys. US Patent 3174851, March 23
7. Li MG, Sun DQ, Qiu XM, Sun DX (2006) Effects of laser brazing parameters on microstructure and properties of TiNi shape memory alloy and stainless steel joint. Mater Sci Eng A 424:17–22
8. Tuissi A, Besseghini S, Ranucci T, Squatrito F et al (1999) Effect of Nd-YAG laser welding on the functional properties of the Ni–49.6 at.% Ti. Mater Sci Eng A 273–275:813–817
9. Shinoda T, Tsuchiya T, Takahashi H (1991) Functional characteristics of friction welded near-equiatomic TiNi shape memory alloy. Trans Jpn Weld Soc 22:30–36
10. Yan XJ, Yang DZ, Liu XP (2007) Corrosion behavior of a laser-welded NiTi shape memory alloy. Mater Charact 58:623–628
11. Hsu YT, Wang YR, Wu SK, Chen C (2001) Effect of CO2 laser welding on the shape memory and corrosion characteristics of TiNi alloys. Metall Mater Trans A 32:569–576
12. Lopez HF, Salinas A (1996) Microstructural aspects of precipitation and martensitic transformation in a Ti-rich Ni-Ti alloy. Scr Mater 34:659–664
13. Borrisutthekul R, Yachi T, Miyashita Y, Mutoh U et al (2007) Suppression of intermetallic reaction layer formation by controlling heat flow in dissimilar joining of steel and aluminum alloy. Mater Sci Eng A 467:108–113
14. Von Allmen M, Blatter A (1995) Laser-beam interactions with materials: physical principles and applications. Springer
15. Tuissi A, Bassani P, Gerosa M, Mauri D, et al. (2003) CO_2 laser welding of NiTi/Ni-based alloys. Proc. Int. Conf. Shape Memory and Superelastic Technologies, Pacific Grove, CA, USA: 229–238
16. Maletta C, Falvo A, Furgiuele F, Barbieri G et al (2009) Fracture behaviour of nickel-titanium laser welded joints. Mater Eng Perform 18:569–574
17. Song YG, Li WS, Li L, Zheng YF (2008) The influence of laser welding parameters on the microstructure and mechanical property of the as-jointed NiTi alloy wires. Mater Lett 62:2325–2328
18. Gugel H, Schuermann A, Theisen W (2008) Laser welding of NiTi wires. Mater Sci Eng A 481–482:668–671
19. Falvo A, Furgiuele F, Maletta C (2008) Functional behaviour of a NiTi welded joint: two way shape memory effect. Mater Sci Eng A 481–482:647–650
20. Tzeng YF (2000) Process characterization of pulsed Nd:YAG laser seam welding. Adv Manuf Technol 16:10–18
21. Kou S (2003) Welding metallurgy. John wiley publication, second edition, USA
22. Squillace A, Prisco U, Ciliberto S, Astarita A (2012) Effect of welding parameters on morphology and mechanical properties of Ti–6Al–4V laser beam welded butt joints. Mater Proc Technol 212: 427–436
23. (1992) ASM handbook, ASM specialty handbook: volume 3. alloys phase diagrams. Metal park, Ohio: 1239